THE JOURNAL OF PHYSICAL CHEMISTRY A
A JOURNAL OF THE AMERICAN CHEMICAL SOCIETY

pubs.acs.org/JPCA

Article

Dipole Switching by Intramolecular Electron Transfer in Single-Molecule Magnetic Complex $[Mn_{12}O_{12}(O_2CR)_{16}(H_2O)_4]$

Dmitry Skachkov,[‖] Shuang-Long Liu,[‖] Jia Chen, George Christou, Arthur F. Hebard, Xiao-Guang Zhang, Samuel B. Trickey, and Hai-Ping Cheng*

Cite This: *J. Phys. Chem. A* 2022, 126, 5265−5272

Read Online

ACCESS | Metrics & More | Article Recommendations

ABSTRACT: We study intramolecular electron transfer in the single-molecule magnetic complex $[Mn_{12}O_{12}(O_2CR)_{16}(H_2O)_4]$ for R = −H, $-CH_3$, $-CHCl_2$, $-C_6H_5$, and $-C_6H_4F$ ligands as a mechanism for switching of the molecular dipole moment. Energetics is obtained using the density functional theory (DFT) with onsite Coulomb energy correction (DFT + *U*). Lattice distortions are found to be critical for localizing an extra electron on one of the easy sites on the outer ring in which localized states can be stabilized. We find that the lowest-energy path for charge transfer is for the electron to go through the center via superexchange-mediated tunneling. The energy barrier for such a path ranges from 0.4 to 54 meV depending on the ligands and the isomeric form of the complex. The electric field strength needed to move the charge from one end to the other, thus reversing the dipole moment, is 0.01−0.04 V/Å.

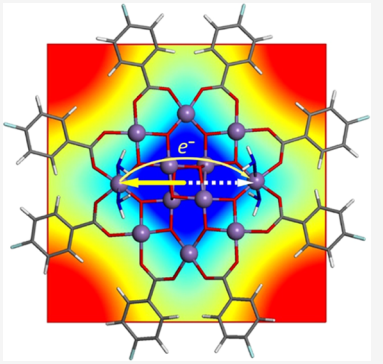

1. INTRODUCTION

$[Mn_{12}O_{12}(O_2CR)_{16}(H_2O)_4]$ (with R = −H, $-CH_3$, $-CHCl_2$, $-C_6H_5$, and $-C_6H_4F$) or "Mn_{12}" for brevity is the prototype single-molecule magnet (SMM). First synthesized in 1980,[1] it is also the first SMM to demonstrate quantum tunneling of magnetization.[2−4] Compared to solid-state magnetic materials, advantages of materials based upon SMMs include small size, perfect monodispersity, low cost, and wide variety of ligands. From a practical point of view, SMMs deposited on a large variety of substrates serve as a prolific platform for prototype device investigation because of their high blocking temperatures and abundant choice of ligands for use in tuning the properties of SMMs.[5−7] SMMs have been considered as candidates for high-density information storage due to the coexistence of electric and magnetic dipoles[2,8−10] and potentially strong magnetoelectric coupling.[11−13] SMMs also have potential applications in high-sensitivity sensors,[14−16] controllable molecular switches for spintronics applications,[17−19] and quantum information processing as qubits.[3,20] Functionality of electronic devices can be achieved by manipulating SMM electronic states by electric field,[21,22] gate voltage,[23] magnetic field,[24] or circularly polarized radiation.[25] Functionality of writing and reading information from SMMs has been demonstrated recently.[21,26]

Switching the dipole moment of an SMM can modify its structural and electronic configuration.[27] There are several dipole-switching mechanisms in different SMMs, including ferroelectric polarization,[28] asymmetric metal electrode screening,[29] carrier trapping/detrapping,[30,31] and dipole−electric field interaction.[32] Intramolecular electron transfer is another way a molecule can switch its dipole moment. In metal−organic and covalent−organic frameworks, metal atoms form metal−oxide columns that work as paths for electron transfer.[33−40] A similar charge-transfer pathway may also exist in Mn_{12}. We suggest that a possible pathway for electron movement from one peripheral Mn atom to another in Mn_{12} may be through the nearest connected oxygen. For synthesizing new complexes and for developing electronic devices based on SMMs, it is very important to know the energy barrier for such electron transfer.

In this work, we use the density functional theory (DFT) with onsite Coulomb energy correction (DFT + *U*) to investigate the intramolecular charge transfer and dipole switching process. First, we show that when Mn_{12} is charged, the added electron is localized on one of the four peripheral Mn atoms, the so-called "easy sites", or on four core Mn atoms. Second, we find the path for moving the electron from a localized location on one easy-site Mn atom to another easy site on the opposite side of the molecule. We show that the lowest-energy path is through the four Mn atoms in the center part (core) of the molecule. The energy barrier for such

Received: April 14, 2022
Revised: July 26, 2022
Published: August 8, 2022

https://doi.org/10.1021/acs.jpca.2c02585
J. Phys. Chem. A 2022, 126, 5265−5272

electron transfer is studied by the nudged elastic band (NEB) method.[41−43] Third, we also study the impact of different ligands on the energy barrier. Finally, we estimate the electric field needed to initiate such an electron transfer process.

The rest of the paper is organized as follows. The Computational Approach section describes our methodology for calculating localized states in an Mn_{12} complex, the energy barrier for electron transfer from one localized state to another, and technical details of calculations. The Results section presents the geometry and electronic configurations of the molecular states studied, the calculated energy barriers for Mn_{12} SMM for the R = −H, $-CHCl_2$, $-CH_3$, $-C_6H_5$, and $-C_6H_4F$ ligands, and the shift of the energy levels as a function of the electric field.

2. COMPUTATIONAL APPROACH

All calculations are based on the DFT as implemented in the Vienna ab initio simulation package (VASP).[44,45] We used the Perdew−Burke−Ernzerhof (PBE) exchange-correlation energy functional[46] and projector-augmented wave (PAW) pseudopotentials.[47] The plane-wave energy cutoff was set to 450 eV. The energy and force convergence tolerances were set to 10^{-8} eV and 0.001 eV/Å, respectively. Phonon calculations were done with the Phonopy package.[48,49] We included 10 Å vacuum between periodic SMMs and incorporated the dipole correction[50,51] for both energy and potential. In the case of charged systems, a uniform background charge (jellium) was assumed to avoid divergence of the total energy.[52] Brillouin zone sampling was via the single Γ point. We used spin-polarized calculations and applied the rotationally invariant DFT + U method[53,54] for Mn d-orbitals with the on-site Coulomb interaction parameter U set to 4 eV. That value produces the correct Mn magnetic moment in such systems.[55,56] The external electric field is modeled by a saw-tooth potential.[57]

The energy barrier for electron transfer from one Mn to another was calculated using the NEB method[41−43] as implemented in VASP. To ensure that the electron remains localized on either side of the barrier along the path, the intermediate images in the NEB method start from the configurations calculated from the conventional two-state model.[58−61] In it, we consider two states for localization of an extra electron on one Mn atom (1) and on another (2), consider the displacement of those atoms according to reaction coordinates using linear interpolation between initial and final positions, and allow all atoms except those two Mn atoms to relax. The NEB calculations then were done using preconverged configurations obtained from the conventional two-state model with fixed two Mn atoms.

We have studied several ligands, R = −H, $-CHCl_2$, $-CH_3$, $-C_6H_5$, and $-C_6H_4F$. The unit cell in the calculation contains one such $[Mn_{12}]^-$ molecule (again, in short-hand notation), compensated by a uniform background charge. This allows us to focus on a single molecule instead of the real crystal structure of the $[Mn_{12}]^-$ complexes, which contains close-packed negatively charged molecules and positively charged counterions.[62−65] Such complexes are computationally much more expensive than the simplified systems considered here since the unit cell contains several SMMs and counterions. The simplified systems nonetheless provide insight into key issues of charge transfer and dipole switching. Another reason to model a separate molecule instead of those close packed in the crystal form is that applying saw-tooth potential with periodic boundary condition (PBC) may disturb the crystal.

3. RESULTS

We start from the electronic configuration of the neutral $[Mn_{12}]^0$ molecule and then consider the electronic configuration for the $[Mn_{12}]^-$ molecule at the negative charge state from having an extra electron. Structural stability is confirmed by the fact that the calculated phonon spectrum has no imaginary frequencies. The section concludes with the calculated energy barrier for electron movement inside the molecule from one Mn atom to another and the electric field needed to initiate electron transfer.

3.1. Neutral $[Mn_{12}]^0$ Complex.

$[Mn_{12}O_{12}(O_2CR)_{16}(H_2O)_4]$ contains 12 Mn atoms, as shown in Figure 1. The first eight Mn atoms (numbered **1**−**8** in Figure 1) are located on the peripheral Mn ring of the molecule. They are in the 3+ charge state, each with four electrons in the 3d-orbitals with a total spin of S = 2 per Mn atom; hence, the total spin of the outer ring is S = 16. The remaining four central Mn atoms (numbered **9**−**12** in the Figure 1) form the molecular core $[Mn_4^{4+}O_4]$. They are in the 4+ charge state.

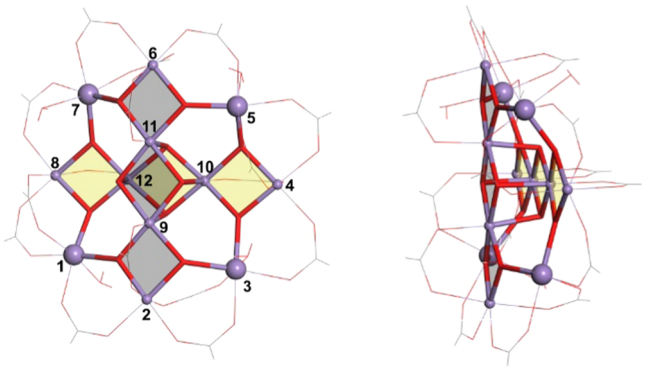

Figure 1. Top view (left) and side view (right) of the Mn_{12} molecule. Chemical bonds are depicted as red-purple bars, with the red end connecting oxygen atoms. Thin lines depict the ligands.

These Mn atoms have three electrons in the 3d-orbitals with a total spin of S = 3/2 per atom. The interaction among them is ferromagnetic; the total core spin of S = 6.[62] Eight of the Mn atoms, comprising all four core Mn atoms and the four peripheral Mn atoms on the hard sites, and their O neighbors form two parallel Mn−O planes highlighted by the gray and yellow areas in Figure 1. The direction perpendicular to those planes is associated with an easy axis of magnetization for the molecule.[62] Peripheral active (easy) Mn atoms, which are favorable sites for localization of an extra electron, are shown by big purple balls (**1**−**3**−**5**−**7**). They are located between the two Mn−O planes. Sixteen ligands are shown in Figure 1, eight around the peripheral ring of eight Mn atoms (connected to atoms **1**−**8**), four in the front (connected to atoms **1**−**8**, **2**−**9**, **4**−**5**, and **6**−**11**) and four in the back (connected to atoms **6**−**7**, **8**−**12**, **4**−**10**, and **2**−**3**) of the molecule. Inelastic scattering experiments[66] show that the magnetic interaction between the Mn_4 core and the Mn_8 ring is antiferromagnetic. Thus, the ground state of the neutral $[Mn_{12}]^0$ complex has a total spin of S = 10. Figure 2 shows the calculated spin distribution of a $[Mn_{12}-H]^0$ molecule.

https://doi.org/10.1021/acs.jpca.2c02585
J. Phys. Chem. A 2022, 126, 5265−5272

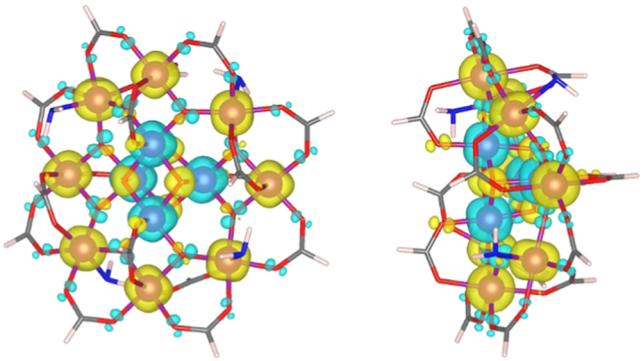

Figure 2. Iso-surface of spin configuration of a $[Mn_{12}{-}H]^0$ SMM, top view (left) and side view (right). Oxygen and carbon atoms are at vertices of red and gray bars, and hydrogen atoms are at the open ends of white bars. Spin iso-surfaces are shown by blue (down) and yellow (up).

Depending upon the various ligand configurations, the four water molecules are absorbed on different Mn sites. Those configurations can be classified as water isomers according to the location of the four adsorbed water molecules. The possible isomer forms are 1:1:1:1, 2:1:1, or 2:2, depending on whether the water molecules are attached to four, three, or two Mn atoms,[63] respectively (see Figure 3). For the 1:1:1:1 configuration, there are three inequivalent Mn atom types, as pointed out by Pederson et.al.[67] In the configuration shown in Figure 1, the water molecules are attached to Mn atoms marked as **1**−**3**−**5**−**7**. For the 2:2 configuration, water molecules may be attached to the **1** and **5** (or **3** and **7**) Mn atoms. Thus, there are four nonequivalent Mn atoms in this isomeric form.

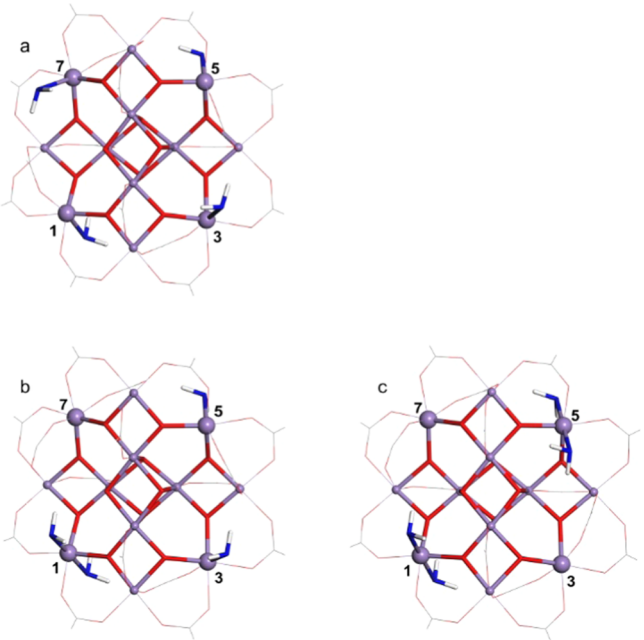

Figure 3. Three water isomers of the Mn_{12} complex. Mn atoms are purple balls with active sites shown as larger balls. Oxygen atoms are at vertices of red bars, and hydrogen atoms are at the open ends of gray bars. Four water molecules, shown as blue-white sticks, can form the (a) 1:1:1:1, (b) 2:1:1, or (c) 2:2 isomers.

For neutral Mn_{12}, all eight peripheral Mn atoms have octahedral oxygen environment with Jahn−Teller (JT) distortion.[62] However, these eight Mn atoms are not equivalent, as shown in Figure 1. The JT elongation axes for Mn atoms on hard sites (**2**, **4**, **6**, and **8**) are parallel to the easy axis of magnetization, whereas the JT elongation axes for Mn atoms on easy sites (**1**, **3**, **5**, and **7**) have significant nonzero angles with respect to the easy axis of magnetization. The Mn atom on an easy site, e.g., atom **1**, is connected to two core Mn atoms, **9** and **12**, through oxygen atoms. This is in contrast to a Mn atom on a hard site, e.g., atom **2**. It is connected to a single core Mn atom, atom **9**, through two oxygen bridges that form a square. The square geometry of the Mn−O−Mn connection for the hard site is more rigid than the six-sided shape for the easy site. Thus, it is easier for the easy site to relax and accommodate an extra localized electron. That difference is also manifested by the fact that the water molecules only attach to the easy sites, as shown in Figure 3.

3.2. Negatively Charged $[Mn_{12}]^-$ Complex. Mn_{12} complexes can accept or lose electrons.[62,63,65] When the SMM molecule charge state is −1; the additional electron localizes on one of the peripheral easy-site Mn atoms. Its charge state is changed from Mn^{3+} to Mn^{2+}. That change can be confirmed experimentally by measuring the elongation of Mn−O bond lengths.[64] In the $[Mn_{12}{-}H]^-$ complex in the 1:1:1:1 isomeric form (shown in Figure 3a), one water molecule is attached to each Mn atom on the easy sites. This form is maintained when an electron is added to the molecule. The Mn−O bond lengths are increased from 1.937 and 1.929 Å for the Mn^{3+} atom (Figure 4a) to 2.183 and 2.139 Å for the Mn^{2+} atom (Figure 4b). In Figures 4 and 5, the significantly changed Mn−O bond lengths caused by accepting an extra electron are highlighted by bold numbers; JT elongation axes are highlighted by yellow lines. Also shown are the energy levels of d-electrons of Mn atoms in an octahedral field with and without JT distortion. In addition to the easy sites on the periphery, our calculations for a single molecule $[Mn_{12}]^-$ in the unit cell with uniform background charge show that Mn atoms from the molecular core also can accept a localized electron. In fact, for an isolated $[Mn_{12}{-}H]^-$ molecule, the resulting state is predicted to be more stable than one which has an electron localizing on one of the peripheral easy sites. We calculated vibrational modes of the $[Mn_{12}{-}H]^-$ molecule with an extra electron localized at either a peripheral easy site or a center site. All vibrational frequencies are real (except for three translational modes), confirming structural stability of both systems. For all studied structures in −1 charge states, the calculated total magnetic moments of SMMs were 21 μ_B.

Figure 4d shows the core Mn atom (marked as **9** in Figure 1) in 4+ charge state, while Figure 4e shows the core Mn atom in 3+ charge state upon acceptance of the extra electron. As pointed out by Christou et al.,[63] a JT distortion is expected for the resulting high-spin Mn^{3+} ion. As may be seen from Figure 4d, the Mn^{4+} atom does not have a JT elongation axis. However, after receiving an extra electron, the Mn−O bonds lengthen (Figure 4e) to form a JT elongation axis perpendicular to the parallel Mn−O planes in Figure 1. That also introduces strain in the rigid $[Mn_4O_4]$ core cubane unit.

With one exception, for all structures studied with an electron located on the core Mn atom, the JT elongation axes of the core Mn atom are perpendicular to the parallel Mn−O planes. The exception is the $-CHCl_2$ ligand. For it, the JT elongation axis for the core Mn atom lies parallel to the planes.

https://doi.org/10.1021/acs.jpca.2c02585
J. Phys. Chem. A 2022, 126, 5265−5272

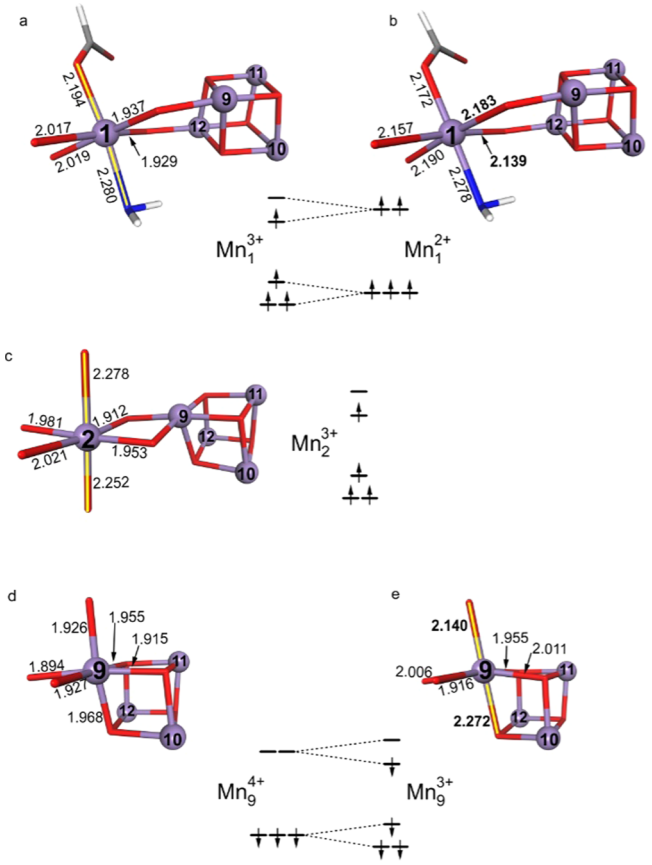

Figure 4. Calculated Mn−O bond length (in Å) for different Mn atoms in the $[Mn_{12}-H]$ complex in 1:1:1:1 isomeric form. Mn atoms are purple balls, oxygen atoms are at vertices of red bars, water molecule as blue-white bars, and carboxylate groups O_2CH as red-gray-white bars. **9**−**10**−**11**−**12** Mn atoms are the core of the complex. **1** Mn atom in 3+ (a) and in 2+ (b) charge states, **2** Mn atom (c), **9** Mn atom in 4+ (d), and in 3+ (e) charge states.

For the other ligands, localizing an extra electron on one of the core Mn atoms becomes less energetically favorable or even unfavorable relative to localizing on one of the easy sites on the peripheral Mn ring due to the strong ligand field (see Table 1). Thus, in contrast to −H and $-CH_3$ ligands, the $-CHCl_2$ ligand localization of an extra electron on the outer ring is energetically more preferable than localization on the core. This fact also confirms the experimental findings that the $[Mn_{12}-CHCl_2]$ SMM is much more effective in attracting electrons than the $[Mn_{12}-CH_3]$.[5]

The Mn atom **2** in the 3+ charge state, shown in Figure 4c, has Mn−O bond lengths identical to those for the Mn atom **1** with the JT elongation axis parallel to the easy axis of magnetization of the molecule. However, this atom cannot accept an additional electron (neither can the equivalent **4**−**6**−**8** atoms) because of the rigid square geometry discussed earlier, so an extra electron initially placed on this atom prefers to move to Mn atoms **1** or **3**.

The 2:2 isomeric form shown in Figure 3c has four water molecules attached to the **1** and **5** easy sites in pairs, thus breaking the symmetry between the **1** and **5** sites and the **3** and **7** sites, with the **3** and **7** sites attached to the ligands instead of water molecules. Our calculations show that an extra electron placed on **1** is energetically more favorable than for placement on **3** by 144 meV. Comparison of the 1:1:1:1 and 2:2 isomeric

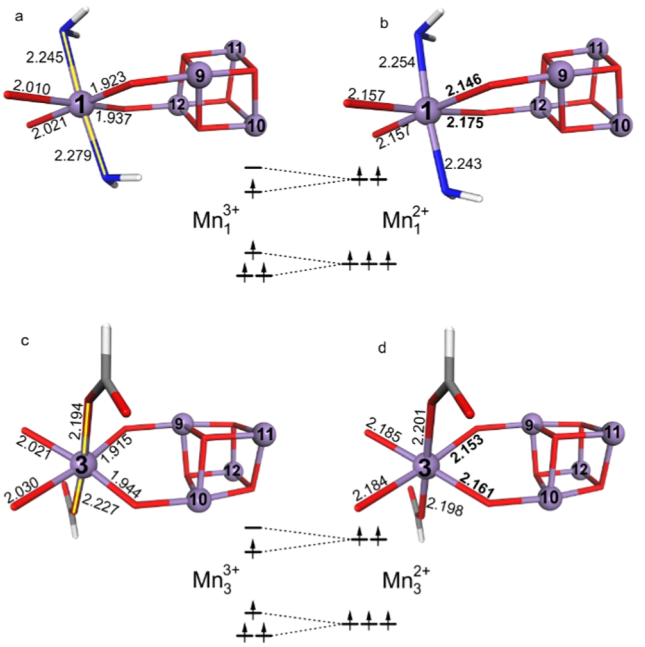

Figure 5. Calculated Mn−O bond lengths (in Å) for **1** and **3** Mn atoms of $[Mn_{12}-H]$ complex in the 2:2 isomeric form. **1** Mn atom in 3+ (a) and in 2+ (b) charge states, **3** Mn atom in 3+ (c) and in 2+ (d) charge states. For details of the figure, see caption in Figure 4.

forms shows that an electron localized on **1** in the 1:1:1:1 form is less stable by 21 meV than for localization on **1** in the 2:2 isomeric form. This means that in the 2:1:1 isomeric form (Figure 3b), localization of an extra electron will be more stable on atom **1**, where two water molecules are attached. In contrast, localization on **3** or **5** will be 21 meV less energetically favorable and localization on **7** will be ≈150 meV less energetically favorable.

3.3. Energy Barrier for Dipole Switching. We consider two pathways for electron transfer, either of which can be the first stage of an electron transfer process that leads to dipole switching. Both pathways start from the easy site **1**. The first pathway involves electron transfer to the nearest possible localization on the easy site of the outer ring (**3**), **1** → **3**. The second pathway is to the nearest Mn atom in the core, **1** → **9**. Table 1 shows the electric dipole moment when the electron is localized on sites **1**, **3**, **5**, **7**, and **9**, the difference in energy for localized states relative to site **1**, and the energy barrier for electron transfer, calculated for an isolated charged $[Mn_{12}]^-$ molecule in a large box with a uniform positive charge background. The dipole moment $\boldsymbol{P}$ is defined as[50,51]

$$\boldsymbol{P} = \int d\boldsymbol{r}(\boldsymbol{r} - \boldsymbol{R}_{\text{center}})\rho_{\text{ions+valence}}(\boldsymbol{r})$$

where $\boldsymbol{R}_{\text{center}}$ is the center of the $[Mn_{12}]^-$ molecule and $\rho_{\text{ions+valence}}$ is the total charge density. As can be seen from Table 1, transferring an electron from **1** to **3** changes the dipole direction, whereas transferring an electron **1** → **9** changes the dipole moment magnitude. In the 1:1:1:1 isomeric form, sites **1** and **3** are equivalent for localization, but in the 2:2 isomers, those two localized states differ by 144−157 meV, depending on the ligand (see Table 1). The state with an electron localized on site **3** in $[Mn_{12}-H]^-$ is higher in energy by 144 meV. Transferring an electron **1** → **3** needs to overcome an energy barrier of 146 meV. Because of this, in the 2:2 isomers, the **1** → **3** pathway is not likely. Figure 6 shows energy profiles

https://doi.org/10.1021/acs.jpca.2c02585
J. Phys. Chem. A 2022, 126, 5265−5272

Table 1. Electron Localization Energy Differences (in meV) Between Outer State 1 and Core State 9, and Between 1 and 3 Outer States, Energy Barriers (in meV) for Electron Transfer From 1 → 3 and 1 → 9, Electric Field for Initiation of Dipole Switching, Slope Coefficients $1/2\delta D$, and Electric Dipole Moment of the States in Mn_{12} Complexes with Different Ligands[a]

ligand	water isomer	energy difference $E_3 - E_1$	energy difference $E_9 - E_1$	energy barrier for 1 → 3	energy barrier for 1 → 9	electric field (V/Å)	$1/2\delta D$ (meV /(V/ Å))	electric dipole moment **P** (in *x*,*y*,*z*) (*e* × Å)				
								1	**3**	**5**	**7**	**9**
−H	1:1:1:1	0	−24	5.3	0.4	−0.034	−808	−1.134	0.242	1.134	−0.242	−0.257
								−0.167	-1.233	0.167	1.233	−0.256
								−0.098	0.150	−0.098	0.150	−0.002
$-CH_3$	1:1:1:1	0	−11	45	19	−0.014	−896	−1.239	0.553	1.239	−0.553	−0.138
								0.565	−1.091	−0.565	1.091	−0.431
								−0.015	0.205	−0.015	0.205	0.357
$-CHCl_2$	1:1:1:1	0	+28	5.8	39	+0.031	−925	−1.541	-0.874	1.541	0.874	−0.668
								−0.759	0.959	0.759	−0.959	−0.009
								0.489	0.342	0.489	0.342	0.177
−H	2:2	+144	+30	146	41	+0.035	−799	−1.223	−0.004	1.223	0.004	−0.349
								−0.011	−1.227	0.011	1.227	−0.216
								−0.096	0.010	−0.096	0.010	−0.154
$-C_6H_5$	2:2	+157	+13	166	54	+0.011	−1098	−1.497	−0.006	1.497	0.006	−0.336
								−0.032	−1.603	0.032	1.603	−0.294
								−0.028	0.111	−0.028	0.111	−0.218
$-C_6H_4F$	2:2	+150	−18	150	36	−0.017	−1090	−1.478	0.023	1.478	−0.023	0.327
								−0.007	−1.576	0.007	1.576	−0.285
								0.133	0.029	0.133	0.029	0.327

[a]For labeling of the atoms see Figure 1. In the 1:1:1:1 isomeric form (Figure 3a), water molecules are attached to **1**, **3**, **5**, and **7** Mn atoms, whereas in the 2:2 isomeric form (Figure 3c), water molecules are attached to **1** and **5** Mn atoms.

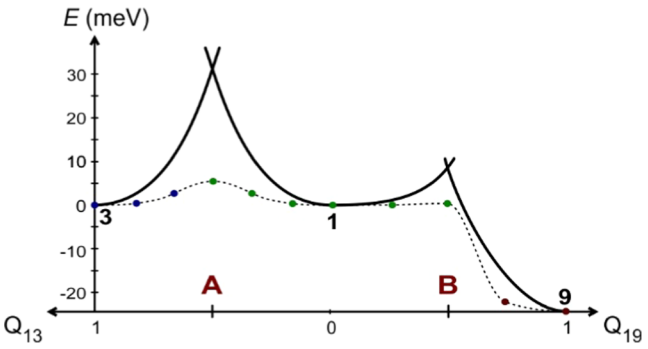

Figure 6. Energy profiles for reactions **1** → **3** and **1** → **9** for $[Mn_{12}-H]^-$ complex in 1:1:1:1 isomeric form using conventional two-state model (solid black lines) and NEB (dashed line). Blue, green, and purple dots correspond to localization of electron on **3**, **1**, and **9**, respectively. Q_{13} and Q_{19} are reaction coordinates.

for paths **1** → **3** and **1** → **9** for the $[Mn_{12}-H]^-$ complex in 1:1:1:1 isomeric form using the conventional two-state model and NEB discussed above. Dots on the NEB curve show several images on the pathway. Displacements **1** → **A** and **1** → **B** correspond to Mn atom shifts to 0.099 and 0.135 Å, respectively. For **1** → **3**, the conventional two-state model gives an energy barrier of 31.1 meV, whereas the NEB method finds a pathway with an energy barrier of 5.3 meV. Transferring an electron from **1** to the core **9** requires the overcoming of an energy barrier of 0.4 meV to move to the lower-energy state and create JT distortion on **9** (see Figure 4e).

3.4. Effect of Electric Fields. Applying an external electric field alters the energetically favorable site on which the extra electron can be localized. This is the basis for dipole switching. Here, we apply an electric field computationally to estimate the strength of an external electric field needed to alter the localization site. The applied electric field is in the plane of easy Mn sites and parallel to the projection of the vector from **1** to **9** onto the same plane. Let E_1 (E_9) be the total energy of $[Mn_{12}]^-$ with the extra electron localized at **1** (**9**). Figure 7

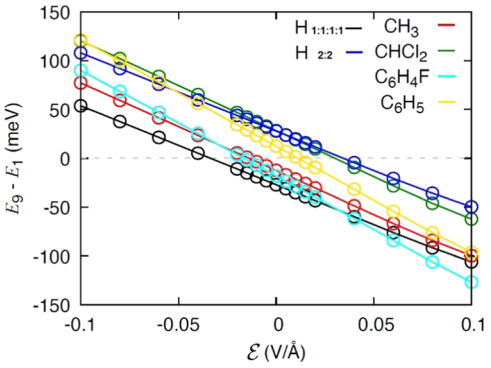

Figure 7. Energy difference due to different location of the extra electron versus electric field.

shows the energy difference $\delta E = E_9 - E_1$ versus electric field strength $\mathcal{E}$. δE changes linearly with $\mathcal{E}$ and reaches zero at $\mathcal{E} = -0.034$ V/Å for $[Mn_{12}-H]^-$. The negative sign of the electric field corresponds to the direction of the field from the center of the molecule to the outside. The sign of the field is defined by the sign of the energy difference $E_9 - E_1$. However, it also indicates the strength of the ligand field. Thus, for $[Mn_{12}-CH_3]^-$ and $[Mn_{12}-H]^-$ complexes in 1:1:1:1 isomeric forms, the electric field direction to align the **1** and **9** states is from the center of the complex to the outer ring, whereas for the $[Mn_{12}-CHCl_2]^-$ complex in 1:1:1:1 isomeric form, the field direction is reversed, indicating significant own-field for the electronegative $-CHCl_2$ ligand. The slope of the δE dependence upon $\mathcal{E}$ (see Figure 7) can be associated with the electric displacement $\boldsymbol{D}$ of the media according to

https://doi.org/10.1021/acs.jpca.2c02585
J. Phys. Chem. A 2022, 126, 5265−5272

$$\delta E = \delta E(0) + \frac{1}{2}\delta D\mathcal{E} = \delta E(0) + \frac{1}{2}\delta P\mathcal{E}$$

where $\delta P = -|\boldsymbol{P}_9 - \boldsymbol{P}_1|$, since $\boldsymbol{D} = \boldsymbol{\varepsilon}_0\boldsymbol{\mathcal{E}} + \boldsymbol{P}$. Thus, the slope of $\delta E(\mathcal{E})$ is proportional to the absolute value of the electric dipole moment: a larger dipole moment of the complex corresponds to a larger slope coefficient. For example, for $[Mn_{12}{-}C_6H_4F]^-$ and $[Mn_{12}{-}C_6H_5]^-$ complexes, the slope coefficients are 1090 and 1098 meV/(V/Å) and dipole moments $|\boldsymbol{P}_1|$ are 1.484 and 1.498 eÅ, respectively, whereas for $[Mn_{12}{-}H]^-$ complexes, the slope coefficients are 808 and 799 meV/(V/Å), respectively and dipole moments $|\boldsymbol{P}_1|$ are 1.150 and 1.227 eÅ. The slope coefficients $1/2\delta D$ are summarized in Table 1. To be sure that our calculation procedure with saw-tooth potential in PBC is valid, we also calculated the electric field when the molecules are separated by 20 Å. The resulting changes in the electric field value are less than 6%.

Calculated values of electric field strengths to initiate the dipole switching process for all of the SMMs studied are in Table 1. We need to point out here that though this field energetically aligns the two states (**1** and **9**), it is not enough to move an electron from one Mn atom to another since doing that also requires overcoming some activation barrier to make displacements on atoms, thus making the JT distortion. However, these calculated values can give some estimation of the actual electric field for dipole switching. Thus, for −H ligand, where the activation barrier is only 0.4 meV, thus much less than the energy difference $E_9 - E_1$ of 24 meV, the actual electric field for electron movement will be very close to 0.034 V/Å.

These calculations consider only isolated $[Mn_{12}]^-$ molecules. In some experiments, however, the molecules are in crystalline form, with counterions in each unit cell.[62−64] The positively charged counterions and $[Mn_{12}]^-$ molecules of such structures impose a crystal electric field upon the $[Mn_{12}]^-$ molecules. We have calculated the crystal electric field imposed on the Mn_{12} molecule in the $[Mn_{12}{-}C_6H_4F]$ crystal with lattice parameters a = 17.41 Å, b = 17.41 Å, and c = 23.87 Å.[64] Both the crystal electric field in the plane $z = c/2$ and the orientation of the $[Mn_{12}]^-$ molecule in the crystal are shown in Figure 8. The field from the periodic counterions and from all other periodic $[Mn_{12}]^-$ molecules is included in the plot, but the field from the ligands of the molecule itself is not included. As can be seen from Figure 8, the Mn_{12} molecule in the crystal is oriented such that the Mn atoms on the easy sites are located at points (corners of the blue square) with minimum possible electric field strength. Thus, the electric field on the easy-site Mn atoms is 0.022 V/Å, whereas on the hard-site atoms it is 0.063 V/Å. The electric field strength on the core Mn atoms is 0.00025 V/Å.

4. CONCLUSIONS

We have studied different possible pathways for dipole switching in the $[Mn_{12}]^-$ SMM complex with diverse ligands. Ligands play an important role in the energy barrier for electron transfer in the various SMM Mn_{12} molecules. We find that the extra electron can be localized on the easy sites of the peripheral Mn ring or any of the four core Mn atoms. For some ligands, localization on one of the core sites is energetically preferable for isolated molecules. Lattice distortions are found to be critical for localizing the extra electron on one of the easy sites of the peripheral ring. We find that the lowest-energy path for charge transfer is for the electron to go through the center via superexchange-mediated tunneling. The energy barrier for dipole switching is between 0.4 and 54 meV depending on the ligands and the isomeric form of the complex. An important semiquantitative finding is the huge range in energy barriers for dipole switching, more than 2 orders of magnitude. We expect this finding to hold up even if the smaller barriers turn out to be strongly sensitive to the particular exchange-correlation functional. The electric field strength needed to move the charge from one end to the other, thus reversing the dipole moment, is 0.01−0.04 V/Å. Parameters for the crystal field and the structures studied are available for download at M^{2}QM' GitHub page.[68]

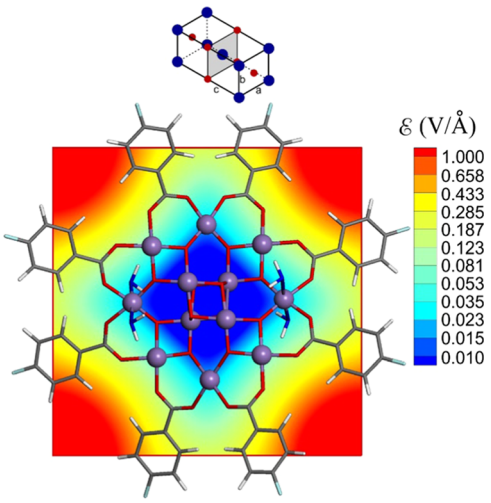

Figure 8. Electric field in the $[Mn_{12}{-}C_6H_4F]$ crystal. The upper part of the figure shows the crystal schematically with blue dots as $[Mn_{12}]^-$, and red dots as positively charged counterions. Mn atoms are purple balls, oxygen and carbon atoms are at vertices of red and gray bars, and hydrogen and fluorine atoms are at the open ends of white and green bars. Four carboxylate groups $O_2C{-}C_6H_4F$ in front and four at the rear of the molecule are removed for clarity.

AUTHOR INFORMATION

Corresponding Author

Hai-Ping Cheng − *The M^{2}QM Center and the Quantum Theory Project, Department of Physics, University of Florida, Gainesville, Florida 32611, United States;* orcid.org/0000-0001-5990-1725; Email: hping@ufl.edu

Authors

Dmitry Skachkov − *The M^{2}QM Center and the Quantum Theory Project, Department of Physics, University of Florida, Gainesville, Florida 32611, United States;* Present Address: NanoScience Technology Center, University of Central Florida, Orlando, Florida 32826, United States; orcid.org/0000-0002-8943-7668

Shuang-Long Liu − *The M^{2}QM Center and the Quantum Theory Project, Department of Physics, University of Florida, Gainesville, Florida 32611, United States;* orcid.org/0000-0003-3253-5491

Jia Chen − *The M^{2}QM Center and the Quantum Theory Project, Department of Physics, University of Florida, Gainesville, Florida 32611, United States;* Present Address: Quantum Simulation Technologies, Inc., Cambridge, Massachusetts 02139, United States; orcid.org/0000-0002-7310-3196

https://doi.org/10.1021/acs.jpca.2c02585
J. Phys. Chem. A 2022, 126, 5265−5272

George Christou − *The M²QM Center, Department of Chemistry, University of Florida, Gainesville, Florida 32611, United States;* orcid.org/0000-0001-5923-5523
Arthur F. Hebard − *The M²QM Center, Department of Physics, University of Florida, Gainesville, Florida 32611, United States*
Xiao-Guang Zhang − *The M²QM Center and the Quantum Theory Project, Department of Physics, University of Florida, Gainesville, Florida 32611, United States;* orcid.org/0000-0003-0092-5006
Samuel B. Trickey − *The M²QM Center and the Quantum Theory Project, Department of Physics, University of Florida, Gainesville, Florida 32611, United States*

Complete contact information is available at: https://pubs.acs.org/10.1021/acs.jpca.2c02585

Author Contributions

‖D.S. and S.-L.L. contributed equally

Notes

The authors declare no competing financial interest.

■ ACKNOWLEDGMENTS

This work was supported as part of the Center for Molecular Magnetic Quantum Materials (M²QM), an Energy Frontier Research Center (EFRC) funded by the U.S. Department of Energy (DOE), Office of Science, Basic Energy Sciences under Award DE-SC0019330. This research used resources of the National Energy Research Scientific Computing Center (NERSC), a U.S. DOE Office of Science User Facility operated under Contract No. DE-AC02-05CH11231. D.S. thanks Dr. Mykhaylo Krykunov for helpful discussion.

■ REFERENCES

(1) Lis, T. Preparation, structure, and magnetic properties of a dodecanuclear mixed-valence manganese carboxylate. *Acta Crystallogr., Sect. B: Struct. Crystallogr. Cryst. Chem.* **1980**, *36*, 2042−2046.
(2) Thomas, L.; Barbara, B. Quantum Tunneling of the Magnetization In Mn_{12}-Ac. *J. Low Temp. Phys.* **1998**, *113*, 1055−1060.
(3) Leuenberger, M. N.; Loss, D. Quantum computing in molecular magnets. *Nature* **2001**, *410*, 789−793.
(4) Zabala-Lekuona, A.; Seco, J. M.; Colacio, E. Single-Molecule Magnets: From Mn_{12}-ac to dysprosium metallocenes, a travel in time. *Coord. Chem. Rev.* **2021**, *441*, No. 213984.
(5) Zhu, X.; Hale, A.; Christou, G.; Hebard, A. F. Electronegative ligands enhance charge transfer to M_{12} single-molecule magnets deposited on graphene. *J. Appl. Phys.* **2020**, *127*, No. 064303.
(6) Gakiya-Teruya, M.; Jiang, X.; Le, D.; Üngör, Ö.; Durrani, A. J.; Koptur-Palenchar, J. J.; Jiang, J.; Jiang, T.; Meisel, M. W.; Cheng, H.-P.; et al. Asymmetric Design of Spin-Crossover Complexes to Increase the Volatility for Surface Deposition. *J. Am. Chem. Soc.* **2021**, *143*, 14563−14572.
(7) Berkley, R. S.; Hooshmand, Z.; Jiang, T.; Le, D.; Hebard, A. F.; Rahman, T. S. Characteristics of Single-Molecule Magnet Dimers $[Mn_3]_2$ on Graphene and h-BN. *J. Phys. Chem. C* **2020**, *124*, 28186−28200.
(8) Natterer, F. D.; Yang, K.; Paul, W.; Willke, P.; Choi, T.; Greber, T.; Heinrich, A. J.; Lutz, C. P. Reading and writing single-atom magnets. *Nature* **2017**, *543*, 226−228.
(9) Castro-Alvarez, A.; Gil, Y.; Llanosa, L.; Aravena, D. High performance single-molecule magnets, Orbach or Raman relaxation suppression? *Inorg. Chem. Front.* **2020**, *7*, 2478−2486.
(10) Shao, D.; Wang, X. Y. Development of single-molecule magnets. *Chin. J. Chem.* **2020**, *38*, 1005−1018.
(11) Yin, L.; Xia, J.-S.; Sullivan, N.; Fry, J.; Cheng, H.-P.; Yazback, M.; Zapf, V. S.; Paduan-Filho, A. Anomalous frequency dependence of magneto-electric effect in doped DTN. *Phys. B* **2021**, *608*, No. 412875.
(12) Jakobsen, V. B.; Chikara, S.; Yu, J.-X.; Dobbelaar, E.; Kelly, C. T.; Ding, X.; Weickert, F.; Trzop, E.; Collet, E.; Cheng, H.-P.; et al. Giant Magnetoelectric Coupling and Magnetic Field-Induced Permanent Switching in a Spin Crossover Mn(III) Complex. *Inorg. Chem.* **2021**, *60*, 6167−6175.
(13) Chikara, S.; Gu, J.; Zhang, X.-G.; Cheng, H.-P.; Smythe, N.; Singleton, J.; Scott, B.; Krenkel, E.; Eckert, J.; Zapf, V. S. Magnetoelectric behavior via a spin state transition. *Nat. Commun.* **2019**, *10*, No. 4043.
(14) Chelebaeva, E.; Larionova, J.; Guari, Y.; Ferreira, R. A.; Carlos, L. D.; Paz, F. A. A.; Trifonov, A.; Guerin, C. Luminescent and magnetic cyano-bridged coordination polymers containing 4d− 4f ions: toward multifunctional materials. *Inorg. Chem.* **2009**, *48*, 5983−5995.
(15) Montgomery, C. P.; Murray, B. S.; New, E. J.; Pal, R.; Parker, D. Cell-penetrating metal complex optical probes: targeted and responsive systems based on lanthanide luminescence. *Acc. Chem. Res.* **2009**, *42*, 925−937.
(16) Yuan, S.; Qin, J.-S.; Lollar, C. T.; Zhou, H.-C. Stable metal−organic frameworks with group 4 metals: current status and trends. *ACS Cent. Sci.* **2018**, *4*, 440−450.
(17) Urdampilleta, M.; Nguyen, N. V.; Cleuziou, J. P.; Klyatskaya, S.; Ruben, M.; Wernsdorfer, W. Molecular quantum spintronics: Supramolecular spin valves based on single-molecule magnets and carbon nanotubes. *Int. J. Mol. Sci.* **2011**, *12*, 6656−6667.
(18) Wang, Z.; Qin, W. Organic magnetoelectric and optomagnetic couplings: perspectives for organic spin optoelectronics. *NPG Asia Mater.* **2021**, *13*, 17.
(19) Coronado, E. Molecular magnetism: from chemical design to spin control in molecules, materials and devices. *Nat. Rev. Mater.* **2020**, *5*, 87−104.
(20) Najafi, K.; Wysocki, A. L.; Park, K.; Economou, S. E.; Barnes, E. Toward Long-Range Entanglement between Electrically Driven Single-Molecule Magnets. *J. Phys. Chem. Lett.* **2019**, *10*, 7347−7355.
(21) Sato, T.; Breedlove, B. K.; Yamashita, M.; Katoh, K. Electro-Conductive Single-Molecule Magnet Composed of a Dysprosium-(III)-Phthalocyaninato Double-Decker Complex with Magnetoresistance. *Angew. Chem., Int. Ed.* **2021**, *60*, 21179−21183.
(22) Thiele, S.; Balestro, F.; Ballou, R.; Klyatskaya, S.; Ruben, M.; Wernsdorfer, W. Electrically driven nuclear spin resonance in single-molecule magnets. *Science* **2014**, *344*, 1135−1138.
(23) Liu, S.-L.; Yazback, M.; Fry, J. N.; Zhang, X.-G.; Cheng, H.-P. Single-Molecule Magnet Mn_{12} on GaAs-supported Graphene: Gate Field Effects From First Principles. *Phys. Rev. B* **2022**, *105*, No. 035401.
(24) Zhang, Z.-Z.; Wang, Y.; Wang, H.; Liu, H.; Dong, L. Controllable Spin Switching in a Single-Molecule Magnetic Tunneling Junction. *Nanoscale Res. Lett.* **2021**, *16*, No. 77.
(25) Maryasov, A. G.; Bowman, M. K.; Fedin, M. V.; Veber, S. L. Theoretical Basis for Switching a Kramers Single Molecular Magnet by Circularly-Polarized Radiation. *Materials* **2019**, *12*, 3865.
(26) Xue, H.-B.; Liang, J.-Q.; Liu, W.-M. Manipulation and readout of spin states of a single-molecule magnet by a spin-polarized current. *Phys. E* **2022**, *138*, No. 115086.
(27) Li, X.-G.; Zhang, X.-G.; Cheng, H.-P. Conformational Electroresistance and Hysteresis in Nanoclusters. *Nano Lett.* **2014**, *14*, 4476−4479.
(28) Garcia, V.; Fusil, S.; Bouzehouane, K.; Enouz-Vedrenne, S.; Mathur, N. D.; Barthelemy, A.; Bibes, M. Giant tunnel electroresistance for non-destructive readout of ferroelectric states. *Nature* **2009**, *460*, 81−84.
(29) Zhuravlev, M. Y.; Sabirianov, R. F.; Jaswal, S. S.; Tsymbal, E. Y. Giant Electroresistance in Ferroelectric Tunnel Junctions. *Phys. Rev. Lett.* **2005**, *94*, No. 246802.
(30) Odagawa, A.; Sato, H.; Inoue, I. H.; Akoh, H.; Kawasaki, M.; Tokura, Y.; Kanno, T.; Adachi, H. Colossal electroresistance of a

$Pr_{0.7}Ca_{0.3}MnO_3$ thin film at room temperature. *Phys. Rev. B* **2004**, *70*, No. 224403.
(31) Shang, D. S.; Shi, L.; Sun, J. R.; Shen, B. G.; Zhuge, F.; Li, R. W.; Zhao, Y. G. Improvement of reproducible resistance switching in polycrystalline tungsten oxide films by in situ oxygen annealing. *Appl. Phys. Lett.* **2010**, *96*, No. 072103.
(32) Yasutake, Y.; Shi, Z.; Okazaki, T.; Shinohara, H.; Majima, Y. Single Molecular Orientation Switching of an Endohedral Metallofullerene. *Nano Lett.* **2005**, *5*, 1057−1060.
(33) Rosi, N. L.; Kim, J.; Eddaoudi, M.; Chen, B.; O'Keeffe, M.; Yaghi, O. M. Rod, Packings and Metal-Organic Frameworks Constructed from Rod-Shaped Secondary Building Units. *J. Am. Chem. Soc.* **2005**, *127*, 1504−1518.
(34) Dietzel, P. D. C.; Morita, Y.; Blom, R.; Fjellvåg, H. An in situ High-Temperature Single-Crystal Investigation of a Dehydrated Metal-Organic Framework Compound and Field-Induced Magnetization of One-Dimensional Metal-Oxygen Chains. *Angew. Chem., Int. Ed.* **2005**, *44*, 6354−6358.
(35) Dietzel, P. D. C.; Panella, B.; Hirscher, M.; Blom, R.; Fjellvåg, H. Hydrogen Adsorption in a Nickel Based Coordination Polymer with Open Metal Sites in the Cylindrical Cavities of the Desolvated Framework. *Chem. Commun.* **2006**, 959−961.
(36) Dietzel, P. D. C.; Blom, R.; Fjellvåg, H. Base-Induced Formation of Two Magnesium Metal-Organic Framework Compounds with a Bifunctional Tetratopic Ligand. *Eur. J. Inorg. Chem.* **2008**, *2008*, 3624−3632.
(37) Bloch, E. D.; Murray, L. J.; Queen, W. L.; Chavan, S.; Maximoff, S. N.; Bigi, J. P.; Krishna, R.; Peterson, V. K.; Grandjean, F.; Long, G. J.; et al. Selective Binding of O_2 over N_2 in a Redox-Active Metal-Organic Framework with Open Iron(II) Coordination Sites. *J. Am. Chem. Soc.* **2011**, *133*, 14814−14822.
(38) Zhou, W.; Wu, H.; Yildirim, T. Enhanced H_2 Adsorption in Isostructural Metal-Organic Frameworks with Open Metal Sites: Strong Dependence of the Binding Strength on Metal Ions. *J. Am. Chem. Soc.* **2008**, *130*, 15268−15269.
(39) Sanz, R.; Martinez, F.; Orcajo, G.; Wojtas, L.; Briones, D. Synthesis of a Honeycomb-Like Cu-Based Metal-Organic Framework and its Carbon Dioxide Adsorption Behavior. *Dalton Trans.* **2013**, *42*, 2392−2398.
(40) Sun, L.; Hendon, C. H.; Minier, M. A.; Walsh, A.; Dinca, M. Million-Fold Electrical Conductivity Enhancement in Fe_2(DEBDC) versus Mn_2(DEBDC) (E = S, O). *J. Am. Chem. Soc.* **2015**, *137*, 6164−6167.
(41) Henkelman, G.; Jóhannesson, G.; Jónsson, H. *Theoretical Methods in Condensed Phase Chemistry, Progress in Theoretical Chemistry and Physics*; Kluwer-Academic Publishers: Dordrecht, The Netherlands, 2000; Vol. 5, p 269.
(42) Jónsson, H.; Mills, G.; Jacobsen, K. W. Nudged Elastic Band Method for Finding Minimum Energy Paths of Transitions. In *Classical and Quantum Dynamics in Condensed Phase Simulations*. Berne, B. J.; Ciccoti, G.; Coker, D. F., Eds.; World Scientific: Singapore, 1998 DOI: 10.1142/9789812839664_0016.
(43) Mills, G.; Jonsson, H. Quantum and thermal effects in H_2 dissociative adsorption: Evaluation of free energy barriers in multidimensional quantum systems. *Phys. Rev. Lett.* **1994**, *72*, 1124−1127.
(44) Kresse, G.; Furthmüller, J. Efficiency of ab-initio total energy calculations for metals and semiconductors using a plane-wave basis set. *Comput. Mater. Sci.* **1996**, *6*, 15−50.
(45) Kresse, G.; Furthmüller, J. Efficient iterative schemes for ab initio total-energy calculations using a plane-wave basis set. *Phys. Rev. B* **1996**, *54*, 11169.
(46) Perdew, J. P.; Burke, K.; Ernzerhof, M. Generalized Gradient Approximation Made Simple. *Phys. Rev. Lett.* **1996**, *77*, 3865.
(47) Blöchl, P. E. Projector augmented-wave method. *Phys. Rev. B* **1994**, *50*, 17953.
(48) Togo, A.; Tanaka, I. First principles phonon calculations in materials science. *Scr. Mater.* **2015**, *108*, 1−5.
(49) Phonopy Package for Phonon Calculations at Harmonic and Quasi-Harmonic Levels, Available on GitHub. https://github.com/phonopy/phonopy.
(50) Neugebauer, J.; Scheffler, M. Adsorbate-substrate and adsorbate-adsorbate interactions of Na and K adlayers on Al(111). *Phys. Rev. B* **1992**, *46*, 16067−16080.
(51) Makov, G.; Payne, M. C. Periodic boundary conditions in ab initio calculations. *Phys. Rev. B* **1995**, *51*, 4014.
(52) Paier, J.; Hirschl, R.; Marsman, M.; Kresse, G. The Perdew−Burke−Ernzerhof exchange-correlation functional applied to the G2-1 test set using a plane-wave basis set. *J. Chem. Phys.* **2005**, *122*, No. 234102.
(53) Dudarev, S. L.; Botton, G. A.; Savrasov, S. Y.; Humphreys, C. J.; Sutton, A. P. Electron-energy-loss spectra and the structural stability of nickel oxide: An LSDA+U study. *Phys. Rev. B* **1998**, *57*, 1505−1509.
(54) Shishkin, M.; Sato, H. DFT+U in Dudarev's formulation with corrected interactions between the electrons with opposite spins: The form of Hamiltonian, calculation of forces, and bandgap adjustments. *J. Chem. Phys.* **2019**, *151*, No. 024102.
(55) Chen, D.-T.; Chen, J.; Li, X.-G.; Christou, G.; Hill, S.; Zhang, X.-G.; Cheng, H.-P. Long-Range Magnetic Exchange Pathways in Complex Clusters from First Principles. *J. Phys. Chem. C* **2021**, *125*, 11124−11131.
(56) Schurkus, H. F.; Chen, D.-T.; O'Rourke, M. J.; Cheng, H.-P.; Chan, G.K.-L. Exploring the magnetic properties of the largest single-molecule magnets. *J. Phys. Chem. Lett.* **2020**, *11*, 3789−3795.
(57) Kunc, K.; Resta, R. External Fields in the Self-Consistent Theory of Electronic States: A New Method for Direct Evaluation of Macroscopic and Microscopic Dielectric Response. *Phys. Rev. Lett.* **1983**, *51*, 686.
(58) Marcus, R. A.; Sutin, N. Electron transfers in chemistry and biology. *Biochim. Biophys. Acta* **1985**, *811*, 265−322.
(59) Newton, M. D. Quantum chemical probes of electron-transfer kinetics: the nature of donor-acceptor interactions. *Chem. Rev.* **1991**, *91*, 767−792.
(60) Subotnik, J. E.; Cave, R. J.; Steele, R. P.; Shenvi, N. The initial and final states of electron and energy transfer processes: Diabatization as motivated by system-solvent interactions. *J. Chem. Phys.* **2009**, *130*, No. 234102.
(61) Voityuk, A. A. Electronic coupling for charge transfer in donor−bridge−acceptor systems. Performance of the two-state FCD model. *Phys. Chem. Chem. Phys.* **2012**, *14*, 13789−13793.
(62) Bagai, R.; Christou, G. The Drosophila of single-molecule magnetism: $[Mn_{12}O_{12}(O_2CR)_{16}(H_2O)_4]$. *Chem. Soc. Rev.* **2009**, *38*, 1011.
(63) Kuroda-Sowa, T.; Lam, M.; Rheingold, A. L.; Frommen, C.; Reiff, W. M.; Nakano, M.; Yoo, J.; Maniero, A. L.; Brunel, L.-C.; Christou, G.; Hendrickson, D. N. Effects of Paramagnetic Ferrocenium Cations on the Magnetic Properties of the Anionic Single-Molecule Magnet $[Mn_{12}O_{12}(O_2CC_6F_5)_{16}(H_2O)_4]$.−. *Inorg. Chem.* **2001**, *40*, 6469−6480.
(64) Fournet, A. D.; Mitchell, K. J.; Wernsdorfer, W.; Abboud, K. A.; Christou, G. Three-Dimensional Ferromagnetic Network of Mn_{12} Single-Molecule Magnets: Subtle Environmental Effects and Switching to Antiferromagnetic. *Inorg. Chem.* **2017**, *56*, 10706−10716.
(65) Solera, M.; Mahalay, P.; Wernsdorfer, W.; Lubert-Perquel, D.; Huffman, J. C.; Abboud, K. A.; Hill, S.; Christou, G. Extending the family of reduced $[Mn_{12}O_{12}(O_2CR)_{16}(H_2O)_x]^{n-}$ complexes, and their sensitivity to environmental factors. *Polyhedron* **2021**, *195*, No. 114968.
(66) Chiesa, A.; Guidi, T.; Carretta, S.; Ansbro, S.; Timco, G. A.; Vitorica-Yrezabal, I.; Garlatti, E.; Amoretti, G.; Winpenny, R. E. P.; Santini, P. Magnetic exchange interactions in the molecular nanomagnet Mn_{12}. *Phys. Rev. Lett.* **2017**, *119*, No. 217202.
(67) Park, K.; Pederson, M. R. Effect of extra electrons on the exchange and magnetic anisotropy in the anionic single-molecule magnet Mn_{12}. *Phys. Rev. B* **2004**, *70*, No. 054414.
(68) https://github.com/m2qm-efrc/.

https://doi.org/10.1021/acs.jpca.2c02585
J. Phys. Chem. A 2022, 126, 5265−5272